Egg volume estimation based on image processing and computer vision

Cedric Okinda, Yuwen Sun, Innocent Nyalala, Tchalla Korohou, Samwel Opiyo, Jintao Wang, Mingxia Shen [*]

College of Engineering, Laboratory of Modern Facility Agriculture Technology and Equipment Engineering of Jiangsu Province, Nanjing Agricultural University, Jiangsu, 210031, PR China

ABSTRACT

In chicken egg production line systems, grading based on vision systems is challenging due to ambient light conditions and egg occlusion problems. This study introduces a depth image-based chicken-egg volume estimation system. Two modes of egg configurations on a sorting line were evaluated; single-egg (no occlusion) and multi-eggs (partially occluded, i.e., simple and complex). Contour curvature analysis and k-closest M-circle-center algorithms were used to segment the occluded eggs. Thirteen regression models based on the egg image (single egg) features were trained. The Exponential Gaussian Process Regression outperformed all the explored models with *RMSE* of 1.175 cm^3 and R^2 of 0.984. The same model estimated the volume of the eggs under partial occlusion at *RMSE* of 1.080 and 1.294 cm^3 for simple and complex, respectively. This introduced system can be applied as an accurate, consistent, fast, and non-destructive in-line sorting technique of chicken eggs in a production line system.

1. Introduction

The global population has been projected at 12.3 billion people by the year 2100 (Gerland et al., 2014), with an estimated increase in food demand by 1.1% per year from 2005 to 2050 (Alexandratos and Bruinsma, 2012). Consequently, and with the growing preference of animal protein, the global consumption of meat and animal products is expected to increase by 1.3% and 1.1% per year, respectively (Alexandratos and Bruinsma, 2012). Eggs are very nutritious and provide a significant amount of protein and choline, making it a common substitute for meat and a versatile ingredient in modern cooking (Lesnierowski and Stangierski, 2018). Hence, an increase in egg demand that has resulted in an increase in the global egg production from 37.4 million metric tons to 80 million metric tons from 1990 to 2017 (Statista, 2019). Chicken eggs are most preferred due to the advantages of chicken keeping over other poultry breeds such as duck, goose, quail, turkey, and ostrich. Thus, chicken eggs are widely used in cookery and many types of dishes throughout the world (John-Jaja et al., 2016). The increased demand for chicken eggs over the years has resulted to large-scale production, which has led to challenges in quality, grading and sorting of eggs in these production systems with reference to cost of labor and processing speed.

In supply chain management, size, and mass of agricultural products influence storage and transportation costs, which ultimately affects sales and marketing (Nyalala et al., 2019). Different regions of the world have adopted different criteria for egg classification and grading based on mass, volume, or both (United Nations, 2010). This is due to eggs being different from other agricultural products, an egg starts to lose its mass as soon as it is laid due to respiration and moisture loss, but the volume remains constant (Soltani et al., 2015). Egg geometric parameters, such as volume and surface area, are the core quality attributes evaluated by consumers. Thus, they are critical in the acceptance of an egg (Soltani et al., 2015). Additionally, these parameters are significant in biological research with reference to egg hatchability, physical quality of eggshell, and internal quality of eggs (Zhang et al., 2016).

The conventional modes of egg mass and geometric parameter determination are manual techniques. Whereby an egg's attributes are determined based on weighing scales, drainage method (Archimedes' principle), and the tape method for mass, volume, and surface area estimations, respectively (Asadi et al., 2012; Zhang et al., 2016). However, these techniques are labor-intensive and expensive in large-scale production, in addition to being intrusive, unhygienic, error-prone, and subjective (Sabliov et al., 2002; Zhang et al., 2016). With the developments in computer vision technology, several studies have reported the application of computer vision systems as non-intrusive, non-destructive, accurate, and fast technique in size and mass estimation

of several agricultural products (Nyalala et al., 2019; Zhang et al., 2016). Machine vision systems have been applied to estimate mass and geometric parameters of tomatoes (Concha-Meyer et al., 2018; Eifert et al., 2006; Nyalala et al., 2019), strawberries (Concha-Meyer et al., 2018; Eifert et al., 2006), mushrooms (Concha-Meyer et al., 2018), axisymmetric fruits (apples, lemon, oranges, and sweet-lime) (Phate et al., 2019; Vivek Venkatesh et al., 2015), tamarillos (Wang and Nguang, 2007), eggs (Asadi et al., 2012; Wang and Nguang, 2007), and cantaloupes (Eifert et al., 2006) to mention a few. The basic concept of machine vision-based estimation systems is the correlation of image object features (2D or 3D) to the real weight, volume, or surface area of the object of interest.

Asadi et al. (2012) introduced a fresh egg mass estimation by correlating 2D image features to the real egg mass based on linear and nonlinear regression models. Similar techniques were applied by Javadikia et al. (2011), Thipakorn et al. (2017), Rashidi and Gholami (2011) and Şalvarci and Ayten (2017). However, an egg's external geometric features can only provide an accurate representation of volume or surface area but not the mass, because egg mass is a function of storage time and ambient temperature (Jin et al., 2011; Soltani et al., 2015). Volume estimation of both irregular and axisymmetric agricultural products have also been reported in several studies based on several methodologies such as Monte Carlo method (Siswantoro et al., 2014), 3D wire-frame model reconstruction (Lee et al., 2006), space curving (Chalidabhongse et al., 2006), lofting technique (Goñi et al., 2007), 3D scanners (Uyar and Erdoğdu, 2009), pappus theorem (Soltani et al., 2015), and 3D reconstruction (Zhang et al., 2016). As much as volume estimation systems based on computer vision have been reported, most of the methods mentioned above were mainly based on 2D visible light-based sensors which are susceptible to variation in ambient light conditions. Additionally, 3D scanner though currently readily available cannot be directly applied in a production line system (Zhang et al., 2016). Furthermore, in a real commercial production line system, products often move through a conveyor as a group rather than as a single object. Therefore, this presents an occlusion problem as a bottleneck in machine vision systems applied in production lines. Splitting of occluded objects is a fundamental process in single object analysis in a multi-object setting such as in harvesting and yield estimation (Pastrana and Rath, 2013; Xu et al., 2013). Splitting techniques of similar touching objects such as cells (Bai et al., 2009; Mao et al., 2006) and grains (Lin et al., 2014; Zhang et al., 2005) have been reported. However, there does not exist any literature on the splitting of touching chicken eggs in a production line setting. Therefore, this study introduces a novel technique to separate touching chicken eggs based on shape information analysis.

To overcome the effect of the variations in ambient light condition (Kongsro, 2014; Okinda et al., 2018), this introduced study applied an infrared (IR) depth sensor to estimate the volume of chicken eggs and performed an initial vital task of splitting of touching eggs to determine the volume of each egg in a clutch of eggs as they move through a production conveyor line. The main objective of this study was to develop a depth image-based system for chicken egg volume estimation, with the specific objectives of developing a robust and efficient touching-eggs (partially occluded) splitting algorithm, and to develop a volume estimation model based on extracted feature variables. The proposed system can be applied as a solution to egg sorting and grading problems.

2. Materials and methods

2.1. Egg samples and image acquisition system

A total of 1500 fresh Brown Chicken Eggs of different sizes obtained from a local market at Pukou District, Nanjing, Jiangsu Province, China, were included in this experiment between November 2018 and April 2019. The eggs were manually inspected to be free from dirt and with no visible damage. Each egg was labeled, then volume determined by the drainage method.

The image acquisition sensor applied in this study was a Microsoft Kinect v2 (Microsoft Corp., Washington, USA) camera having a color channel (for observation and data labeling and verification) with a resolution of 1920×1080 pixels and a depth channel (for the proposed system development) with a resolution of 512×424 pixels. The depth channel was selected for system development due to its property of being invariant to variations in ambient light conditions. (Nyalala et al., 2019; Okinda et al., 2018). Hence, no additional illumination was required during image acquisition. The camera was installed 0.80 m perpendicularly above the center of a scanning stage (area within the field of view on a sorting line lane), as shown in Fig. 1. The summary of the Kinect V2 camera properties are presented in Table 1.

The Kinect camera was connected via a USB port to a Microsoft Windows 10 PC (intel core i5-4500U CPU, 4 GHz, 16 GB (Intel, Santa Clara, CA, USA)) pre-installed with Kinect for Windows Software Development Kit (SDK). Both depth and color images were acquired simultaneously by the Kinect camera using MATLAB R2018a (The MathWorks Inc., Natick, MA) at 10 frames per minute (fpm). The data was stored to a 1 TB solid-state drive (SSD) external storage for subsequent analysis.

The labeled egg samples were placed on the scanning stage (0.30 m by 0.30 m) during image acquisition with their axis of rotation parallel to the scanning stage. Two modes of image acquisition were performed described by the eggs' configuration on the scanning stage, as shown in Fig. 2; (a) Images of single eggs (for model development) captured at five different locations on the scanning stage (scanning stage vertices and center location) (*Mod*1). (b) Images of partially occluded eggs. Based on the study by Lin et al. (2014), two kinds of partial occlusions were investigated, i.e., simple touching (eggs touching only on their sides with no holes between them) (*Mod*2) and complex touching (eggs touching each other so closely, randomly and with holes between them) (*Mod*3). A total of 7500 images were captured in *Mod*1(five images per egg). The clutch sizes in *Mod*2 and *Mod*3 were increased from 3 to 15 eggs per image (number of eggs in each clutch was increased by 1 egg from a clutch of 3 till 15 eggs per clutch). A total of 350 images (205 eggs) were captured for each touching configuration (eggs forming different patterns as in Figs. 2 and 9).

All experiments were carried out in Nanjing Agricultural University facilities, in compliance with and using protocols approved by the Biosafety Committee of Nanjing Agricultural University in the handling of agricultural foods and products.

2.2. Image pre-processing and volume estimation model

The main aim of this study was to develop an automatic segmentation and volume estimation system for an egg under both no and partial occlusions. Firstly, eggs in *Mod*1 were used to develop a volume estimation model based on extracted features by image analysis on pre-processed depth images. Secondly, an egg-splitting technique based on curvature analysis was applied to *Mod*2 and *Mod*3. Thirdly, the volume of the split eggs (after splitting) was estimated based on the initially developed model (the model developed in the first step).

The performance of the egg-splitting algorithm was evaluated based on the observed number of eggs in a clutch of eggs against the number of image objects (count) after splitting, computational complexity (time taken to split a clutch of partially occluded eggs), and a comparison in terms of the accuracy of the estimated volume after splitting against the measured volume by the drainage method. Fig. 3 presents the algorithm flow diagram of the proposed chicken-egg volume estimation system.

2.2.1. Image preprocessing algorithm

All raw depth images were processed according to the following procedure. Firstly, based on distance intensities of the depth images (Jana, 2012; Okinda et al., 2018), minimum and maximum thresholds
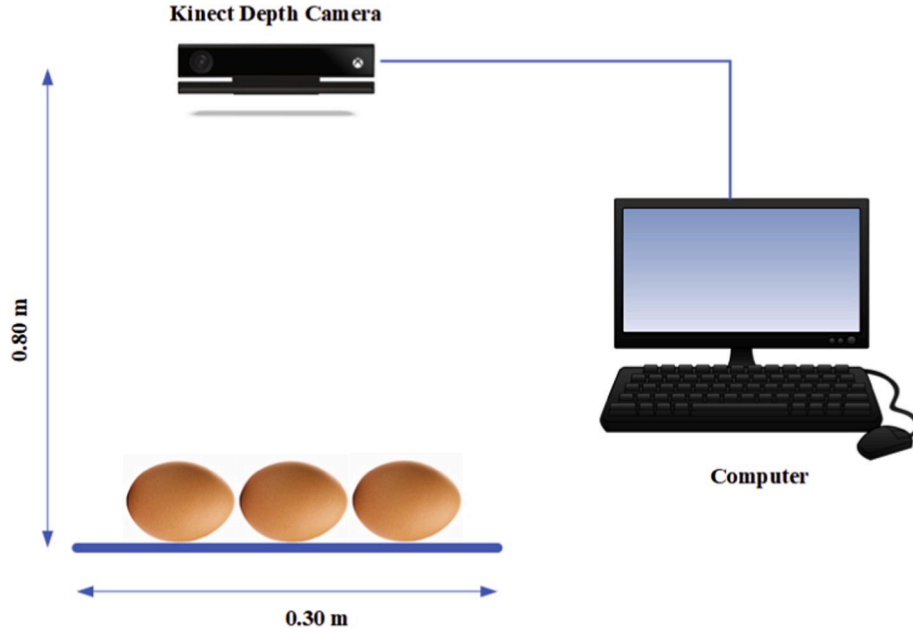
Kinect Depth Camera

Fig. 1. Image acquisition system.

Table 1
Kinect V2 camera specifications (Fankhauser et al., 2015).

Features	Kinect v2 camera	
	Infrared/depth channel	Color channel
Resolution	$512 \times 424 \times 16$ bit per px	$1920 \times 1080 \times 16$ bit per px
Field of view (h x v)	$70.5^0 \times 60.0^0$	$84.1^0 \times 53.8^0$
Angular resolution	0.14^0 per px	–
Operating range	0.5–4.5 m	–
Frame rate	30 Hz	
Latency	~50 ms	
Dimensions ($l \times w \times h$)	$249 \times 66 \times 67$ mm	
Shutter type	Global shutter	

Where h is horizontal, v is vertical, l is length, w is width, h is height, and px is pixel.

(Eq. (1)) were set to segment the Region of Interest (ROI).

$$I_{x,y} = \begin{cases} D_{x,y}, if\ \tau_n \leq D_{x,y} \leq \tau_x \\ 0, \qquad otherwise \end{cases} \qquad (1)$$

where $I_{x,y}$ is the resultant depth image after depth distance threshold, τ_n and τ_x are the minimum and maximum distance thresholds. Secondly, a smoothening operation was performed by a 5 by 5 pixel zero-mean Gaussian kernel filter (Eq. (2)).

$$H_{x,y} = [I_{x,y}] \otimes \omega_{s,t} \qquad (2)$$

where, $H_{x,y}$ is the resultant smoothened image, $\omega_{s,t} = \frac{1}{2\pi\sigma^2}e^{-\frac{1}{2}\left(\frac{s^2+t^2}{\sigma^2}\right)}$ is the Gaussian filter kernel. Thirdly, the morphological opening operation was performed by a disk structural element of size 6 pixels to remove holes in the image object (Eq. (3)).

$$A_{x,y} = H_{x,y} \cdot Se = (H \oplus Se) \ominus Se = \cup \{(Se)_z | (Se)_z\} \qquad (3)$$

where, $A_{x,y}$ is the resultant image after morphological opening, Se is the structural element, and z is the translation.

2.2.2. Volume estimation model

To estimate the volume of an egg, thirteen regression models were explored: Support Vector Regression (SVR) (Linear, Quadratic, Cubic, Fine Gaussian, Medium Gaussian and Coarse Gaussian), Gaussian Process Regression (GPR) (Rational Quadratic, Squared Exponential, Matern 5/2, and Exponential) and Artificial Neural Networks (ANN) (Levenberg-Marquardt, Bayesian Regularization, and Scaled Conjugate Gradient training algorithms). The entire dataset (7500 images) was divided into training (70%) and testing dataset (30%). The image selection criteria for feature extraction was based on manual selection of images under the condition that the eggs do not touch the image edge due to rolling during image acquisition. The models were developed based on the extracted features by performing a 10-fold cross-validation-based parameter search on the training dataset.

2.2.2.1. Features extraction.
The accuracy of any model greatly depends on the feature variables applied in the model training phase. Due to the static position of both the egg and the camera, a full 3D model of the egg was not possible. Therefore, the acquired depth information was only applied to improve the segmentation process (Jun et al., 2018). For each image in *Mod*1, an ellipse was fitted by Direct Least Square method (Halır and Flusser, 1998), after which the fitted ellipse's 2D features i.e., area (γ_A), eccentricity (γ_E) and perimeter (γ_P) were extracted. $\gamma_E = \frac{\lambda_1}{\lambda_2}$ is the ratio of the Eigen values (λ_1 and λ_2) of the covariance matrix of a fitted ellipse (Nyalala et al., 2019; Okinda et al., 2019). γ_P is the number of pixels forming a closed contour of a 2D object. If the close contour has N vertices, the contour can be described as $C = \{(x_n, y_n)\}$, where $n = 1, 2, ..., N$ and $(x_1, y_1) = (x_N, y_N)$, then γ_P can be described by Eq. (4).

$$\gamma_P = \sum_{n=1}^{N-1}(x_{n+1}, y_{n+1}) - (x_n, y_n) \qquad (4)$$

γ_A(Eq. (5)) also known as the projected area (number of pixels in an image object) is a feature that has been widely applied in volume and mass estimation on several agricultural products (Nyalala et al., 2019).

$$\gamma_A = \frac{1}{2}\sum_{n=1}^{N-1}(y_{n+1}x_n - x_{n+1}y_n) \qquad (5)$$

In this study, no feature selection was performed, all the extracted features were applied in the models training and validation process.

2.2.2.2. Regression models.
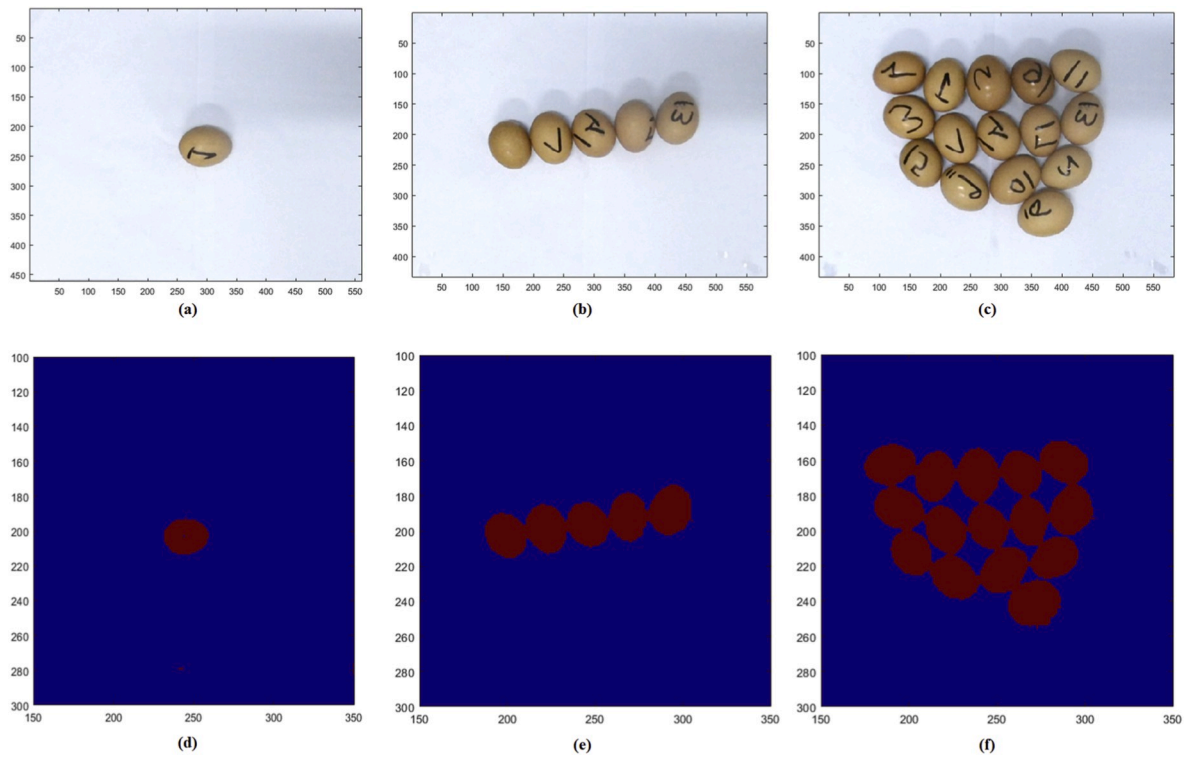The GPs are probabilistic techniques that

Fig. 2. The egg configurations on the scanning stage during image acquisition in color and depth images, (a) and (d) image of a single egg for model development (*Mod*1), (b) and (e) simple touching configuration (*Mod*2), and (c) and (f) complex touching configuration (*Mod*3). (For interpretation of the references to color in this figure legend, the reader is referred to the Web version of this article.)
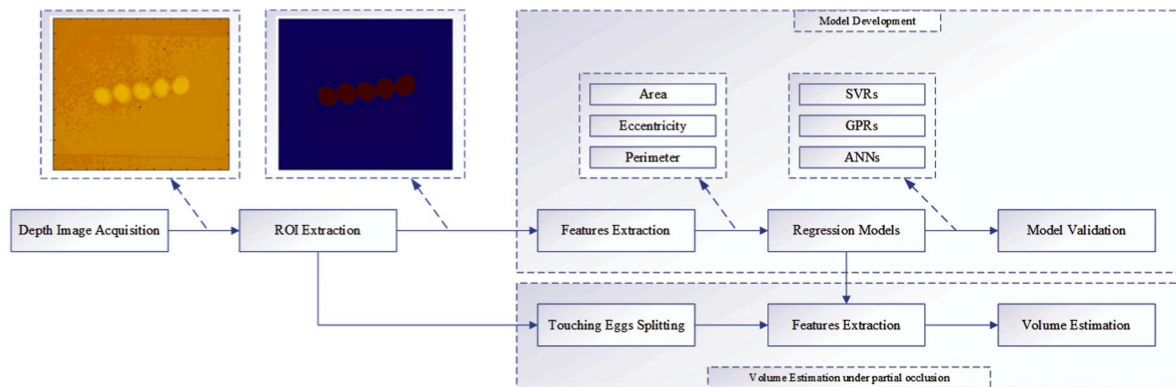

Fig. 3. The algorithm flow diagram of the proposed system.

have been widely applied in regression and classification problems due to their simplicity and flexibility attributes (Quinonero-Candela et al., 2007). From the definition of GPs as a collection of random variables, any finite number having a consistent joint Gaussian distribution, GPR allows a Bayesian use of kernels in the training phase by assuming a GP prior over functions (Williams and Rasmussen, 2006). The GP prior's covariance is specified by passing a positive semi defined kernel object whose hyperparameters are optimized during model fitting by maximizing the log-marginal-likelihood function (Williams and Rasmussen, 2006). The basic GPR kernel functions explored in this study are Squared Exponential (Eq. (6)), also known as Radial-basis function, Matérn 5/2 (Eq. (7)), Rational quadratic (Eq. (8))., and Exponential (Eq. (9)).

The SVR is an extension of the Support Vector Machines (SVMs) to solve regression problems. The SVR models analogously depend only on a subset of the training dataset because the cost function during model development does not consider the training points that lie beyond the margin, thus, easily avoids overfitting (Cortes and Vapnik, 1995).

Generally, an SVR is a quadratic programming problem (QP) aimed at separating support vectors from the rest of the training data vectors (Cortes and Vapnik, 1995). This QP is solved by the kernel functions that map data input into the required forms. Therefore, the choice of the kernel function is a critical factor in the overall performance of an SVR model. The kernel functions applied in this study were Linear (Eq. (10)), Polynomial (Eq. (11)), and Gaussian (Eq. (12)). Table 2 presents a summary of all the GPR and SVR kernel functions explored in this study.

The ANNs are non-linear statistical models whose learning process is a function optimization problem in determining the optimum network parameters to minimize network error (Samarasinghe, 2016). The learning problem in an ANN is the minimization of a loss function by an optimization algorithm. The training of an ANN stops when a specified condition or a stop criteria is satisfied by the optimization algorithm (Samarasinghe, 2016). These optimization (training) algorithms differ in terms of memory complexity, precision, and speed. This study explored three ANNs; each was a 1-hidden layer feed-forward network

Table 2
The GPR and SVR kernel properties descriptions.

Model parameters	kernel equations
Gaussian Process Regression	
Squared exponential	$k_{Se}(r) = exp\left(-\dfrac{r^2}{2\lambda^2}\right)$ (6)
Matérn 5/2	$k_{mt=\frac{5}{2}}(r) = \left(1 + \dfrac{\sqrt{5}r}{\lambda} + \dfrac{5r^2}{3\lambda^2}\right) exp\left(-\dfrac{\sqrt{5}r}{\lambda}\right)$ (7)
Rational quadratic	$k_{Rq}(r) = \left(1 + \dfrac{r^2}{2\alpha\lambda^2}\right)^{-\alpha}$ (8)
Exponential	$k_{Ex}(r) = \exp\left(-\dfrac{r}{\lambda}\right)$ (9)
Support Vector Regression	
Linear	$k_l(x_i, x_j) = x_i^T, x_j$ (10)
Polynomial	$k_Q(x_i, x_j) = \left(1 + x_i^T, x_j\right)^d \quad, d > 0$ (11)
Gaussian	$k_G(x_i, x_j) = exp\left(-\dfrac{x_i - x_j^2}{2\sigma^2}\right) \quad, \sigma > 0$ (12)

Where λ is the characteristic length-scale and r is the Euclidean distance magnitude between the feature vectors x_i, x_j, α is the scale mixture parameter, d is the degree of the polynomial function, and σ is the dimensional feature-space scale.

trained by backpropagation algorithms (Levenberg-Marquardt, Bayesian Regularization, and Scaled Conjugate Gradient training algorithms) activated by Tangent sigmoid function.

2.3. Egg splitting algorithm

In an object recognition problem, the main idea is to extract a feature set discriminating and describing a ROI from the whole image. The main problem is to measure shape similarities by performing shape matching between shape instances to a reference shape (Guerrero-Peña and Vasconcelos, 2017). In touching-eggs condition, an egg is partially occluded by other eggs. Hence, the shape contour may contain occlusions. Thus, resulting in a partial shape matching problem. However, partial shape matching is a challenging task because the location, size, and the number of matched contours may be unknown (Guerrero-Peña and Vasconcelos, 2017). Various non-templet matching techniques based on splitting algorithms have been proposed and applied in object recognition to split similar partially occluded objects (Bai et al., 2009; Lin et al., 2014; Mao et al., 2006; Zhang et al., 2005).

Because an egg is always elliptical, this study proposes a robust multi-ellipse-fitting technique based on contour analysis, the features of each fitted ellipse were then extracted and applied as the input to the volume estimation model. The proposed technique was based on contour fragmentation to eliminate the effects of contour noise (Latecki and Lakämper, 1999; Wang et al., 2014), and extraction of concave and convex points based on contour primitives instead of the whole contour to improve the ellipse fitting performance and computation complexity during the multi-ellipse fitting process.

2.3.1. Contour pre-processing

Shape-based object analysis is often more preferred to texture base analysis because of its stability against sensor noise (Wang et al., 2014). Contour-based shape representations have been validated as powerful shape description techniques because they can represent both structural and global shape information (Wang et al., 2014; Zhang and Lu, 2004). However, as already mentioned, contour noise often affects the performance of contour-based algorithms. Therefore, noise and other extraneous information on a contour need to be eliminated while preserving the crucial parts of the contour (Wang et al., 2014). Contour fragmentation techniques such as dense sampling (Sun and Super, 2005) and discrete contour evolution (DCE) (Latecki and Lakämper, 1999) have always been performed to remove contour noise by dividing the contour into primitives.

Consider the 2D binary image $A_{x,y}$ is described by its contour feature-set $C_{x,y}$ represented by $S(t) = [x(t), y(t)]$, where $t \in [0, 1]$. A simplified polygon $(P_{x,y})$ on $C_{x,y}$ with vertices $\overrightarrow{u} = (u_1, u_2, ..., u_n)$ was obtained by the DCE technique, where, n is the number of vertices. $\overrightarrow{u}$ are the critical points on S (marked by yellow stars in Fig. 4). Finally, the primitives of $C_{x,y}$, $Cp(S)$ are extracted between all pairs of critical points (u_i, u_j) as given in Eq. (13).

$$Cp(S) = \left\{c_{ij} = \left(u_i, u_j\right)\right\} \qquad i \neq j, i, j \in [1, ..., n] \qquad (13)$$

where, c_{ij} is a contour primitive between u_i and u_j. It is worth knowing that u_i and u_j do not have to be adjacent and also $S = c_{ij} \cup c_{ji}$. Note that, for *Mod*2, there is only one contour (outer contour). However, for *Mod*3, there are two contours (outer and inner contours), as shown in Fig. 4. Hence, DCE was applied on both inner and outer contours in the *Mod*3.

2.3.2. Concave and convex points extraction

The use of polygon vertices is often more accurate in determining the convex (C_x) an concave (C_v) points as opposed to contour points (Laiche et al., 2014). Therefore, C_v and C_x points can be determined by the internal angle between two intersecting vectors (vertex). Considering that $C_{x,y}$ is presented by $\overrightarrow{u} = P_{x,y} = \{(x_1, y_1), (x_2, y_2), ..., (x_n, y_n)\}$ polygon vertices. The vectors are then represented by $\overrightarrow{G}_n = [(x_n - x_{(n-1)}, y_n - y_{(n-1)})]$ for the nth vector. Hence, C_v and C_x points of the extracted cp_n are determined according to Eq. (14) based on the sign of the determinant, which signifies the oriented area of a parallelogram generated by the two vectors.

$$u_n = \begin{cases} convex & if \det[\overrightarrow{G}_{(n-1)} : \overrightarrow{G}_n] > 0 \\ concave & otherwise \end{cases} \qquad (14)$$

For *Mod*2, only the C_v was extracted. However, for the *Mod*3, both C_v and C_x points were extracted for the outer and inner contour points, respectively, as shown in Fig. 5 (red stars and white stars represents the C_v and C_x points on the outer and inner contours, respectively).

2.3.3. Split-line extraction

The C_v and C_x points were then used to draw the splitting line in the image (splitting of two partially occluded eggs). For the *Mod*2, the k-nearest neighbors (KNN) nearby search (Friedman, 2018) for each C_v point was performed to find its corresponding C_v point. However, for the complex touching configuration, splitting was performed in three steps. Firstly, the KNN nearby search was performed for each C_v point to find their corresponding C_v points based on a Euclidian distance threshold (ξ) between the points. If the Euclidian distance between a point C_{vi} and its neighbor C_{vj} was greater than ξ, then the points were not considered as neighbors (red split-lines label A in Fig. 6). Secondly, another KNN nearby search was performed on the remaining C_v points to find their corresponding C_x points (cyan split-lines label B in Fig. 6). Lastly, another KNN nearby search was performed on each of the remaining C_x points to find their corresponding C_x neighbors based on ξ(magenta split-lines label C in Fig. 6). Basically, KNN nearby search is performed
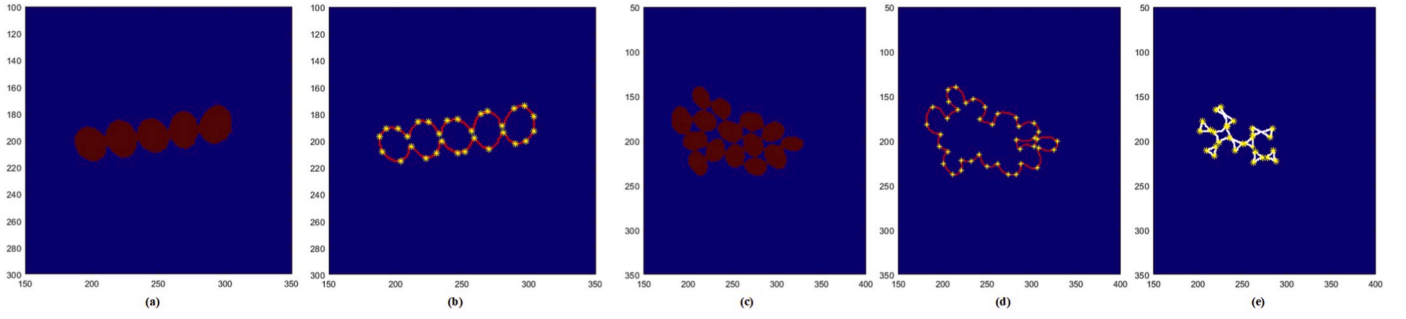
Fig. 4. The contour pre-processing by DCE on the contours of partially occluded eggs images, (a) preprocessed depth image of simple touching configuration (*Mod2*), (b) extracted critical points on the contour of simple touching configuration (*Mod2*), (c) preprocessed depth image of complex touching configuration (*Mod3*), (d) extracted critical points on the outer contour of complex touching configuration (*Mod3*), and (e) extracted critical points on the inner contour of complex touching configuration (*Mod3*).
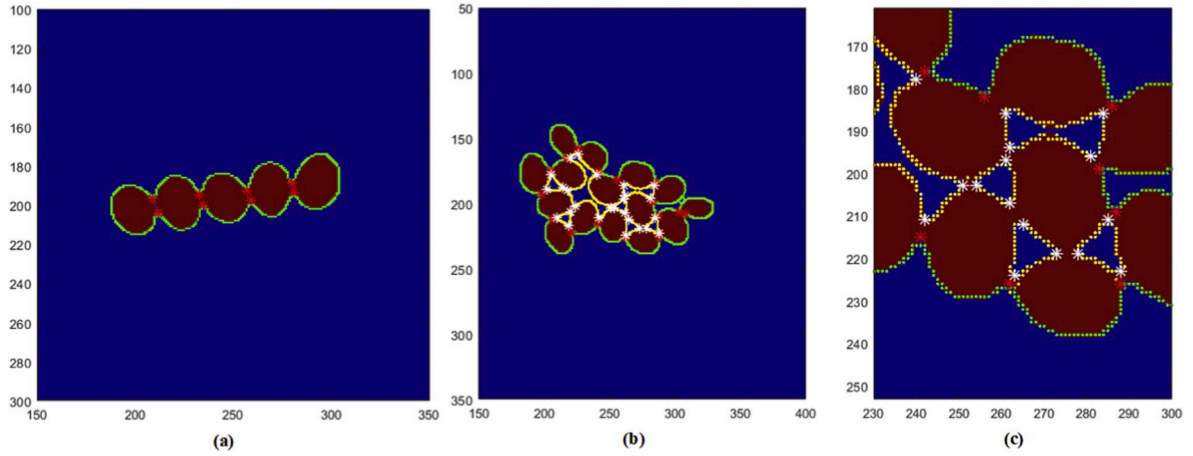

Fig. 5. The extraction of concave and convex points on (a) simple touching configuration (*Mod2*), (b) complex touching configuration (*Mod3*), and (c) a zoomed image of (b) the red stars and white stars represents the concave and convex points on the outer and inner contours, respectively. (For interpretation of the references to color in this figure legend, the reader is referred to the Web version of this article.)
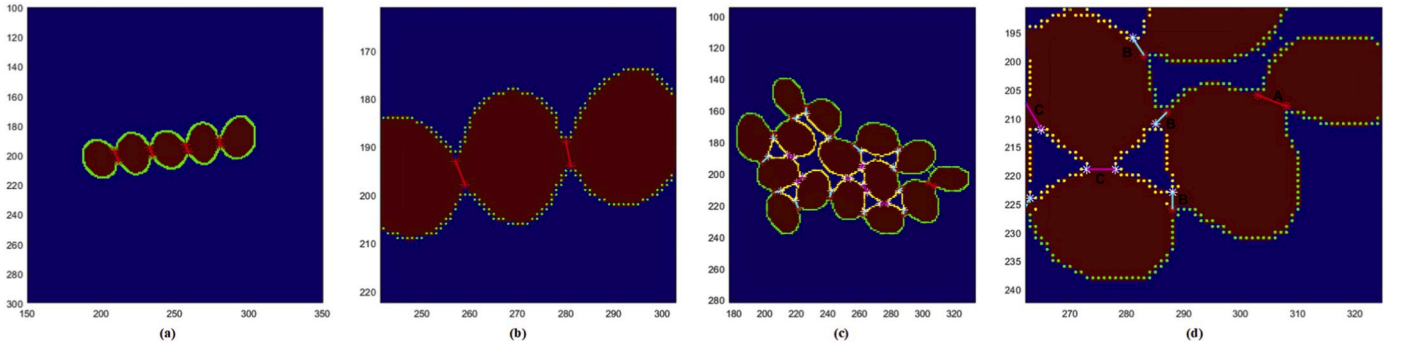

Fig. 6. The split-lines extraction to separate the touching eggs in (a) simple touching configuration (*Mod2*) and (c) complex touching configuration (*Mod3*). (b) and (d) zoomed images of (a) and (c), respectively.

as follows, consider that a point C is uniquely associated with another point $C_j \in P_{x,y}$(nearest) with reference to the Euclidian distance between them the nearest neighbor of C is computed according to Eq. (15).

$$[C, C^*] = argmin_{C, C_j \in P_{x,y}} \ KNN\{C_j : (C_i, C_j) \in P_{x,y}\} \qquad i = 1, 2, \dots j \quad (15)$$

where C^* is the computed nearest neighbor of C. For each C_v and C_x points and their corresponding neighbors, a split-line was drawn to join the two points, as shown in Fig. 6. Hence, separating two touching eggs.

2.3.4. Ellipse modeling by center-based clustering

Consider that the number of objects in $A_{x,y}$ after inserting the split-lines are clusters (c), then the boundary point for each c is the data points from k ellipses that are to be fitted (Marošević and Scitovski, 2015). The boundary of all the c in $A_{x,y}$ can be defined by a dataset $\mathscr{C} = \{a = (x,y) \in \mathbb{R}^2 : i = 1, \dots, m\} \subset \mathbb{R}^2$. Each c boundary is a disjointed subset of $\mathscr{C}$. Therefore, $\mathscr{C}$ is segmented into k subsets $\pi_1, \dots, \pi_k, 1 \leq k \leq m$, such that $\cup_{j=1}^{k} \pi_j = \mathscr{C}$. Hence, each c boundary can be denoted by $\prod(\mathscr{C}) = \{\pi_1, \dots, \pi_k\}$. This basically explains that the elements in $\mathbb{R}^2$ are clustered into k partitions denoted by $\mathscr{P}(\mathscr{C}; k) = \pi_j \in \prod(\mathscr{C})$.

The ellipse representation E_j^* for each cluster is then defined by a global optimization problem as given in Eq. (16). Where $d(p, E)$ is the distance from a point p to an ellipse E, where $E \subset \mathbb{R}^2$.

$$E_j^* \in argmin \sum_{p \in \pi_j} d(p, E) \tag{16}$$

Based on the study by Marošević and Scitovski (2015) an ellipse for each c can be defined by a Mahalanobis circle (M-circle) by introducing the Mahalanobis distance like function $d_M^j : \mathbb{R}^2 \times \mathbb{R}^2 \rightarrow \mathbb{R}_+$ for the jth cluster π_j defined by Eq. (17) (Marošević and Scitovski, 2015).

$$d_M^j(u, v; S_j) = \sqrt{NS_j \left((u - v)^T S_j^{-1} (u - v) \right)} \tag{17}$$

where S_j is a covariant matrix (Eq. (18)) defining the minor and major axis lengths and the orientation of the jth ellipse, c_j (Eq. (19)) is the centroid of the jth cluster π_j, $\sqrt{NS_j}$ is a normalization factor, and $x \in \mathbb{R}^2$

$$S_J = \frac{1}{|\pi_j|} \sum_{p_i \in \pi_j} \left((p_i - c_j)(p_i - c_j) \right)^T \tag{18}$$

$$c_j = argmin \sum_{p_i \in \pi_j} d_M^j(p, x; S_J) = \frac{1}{|\pi_j|} \sum_{p_i \in \pi_j} p \tag{19}$$

If $E_J(c_j, r_j; S_j)$ is an M-circle in the jth cluster π_j, then the algebraic distance from a point $p \in \mathscr{C}$ to the M-circle $E_J(c_j, r_j; S_j)$ of radius r_j at center c_j can be computed by Eq. (20).

$$d(p, E_J(c_j, r_j; S_J)) = \left(d_M^j(p, c_j; S_j) - r_j^2 \right)^2 \tag{20}$$

Therefore, the corresponding cluster center c_j (M-circle-center) for cluster π_j is the solution to a global optimization problem given in Eq. (21). Where $c_j \in \mathbb{R}^2$, $r_j \in \mathbb{R}_+$, $S_j \in \mathbb{R}^{2 \times 2}$, and ψ_j is the sum of the algebraic distances from $p \in \pi_j$ to M-circle $E_J(c_j, r_j; S_J)$.

$$argmin \, \psi_j(c_j, r_j; S_J) = \sum_{p_i \in \pi_j} \left(d_M^j(p, c_j; S_J) - r_j^2 \right)^2 \tag{21}$$

This entire process is considered as The Mahalanobis k-means referred to as the k closest M-circle-centers algorithm (KCMC) (Marošević and Scitovski, 2015) aiming at providing a local optimum partition.

2.3.4.1. KCMC initialization. The initialization of any data clustering algorithm is a trivial process that affects the performance of the entire system. Therefore, an appropriate initial approximation must be defined

for each cluster (M-circle-center). Let the j^{th}M-circle $E_j = \{x \in \mathbb{R} : d_M^j(x, \overline{c}_j; \overline{S}_j) - \overline{r}_j^2\}$ then c_j is the approximation of the centroid $\overline{c}_j$ of the M-circle-center, and $\overline{S}_j$ as the covariance matrix. If $\overline{c}_j$ and $\overline{S}_j$ are known then r_j can be computed by Eq. (22) which is the initial approximation of $\overline{r}_j$.

$$r_j = argmin \sum_{p_i \in \pi_j} \left(d_M^j(p, \overline{c}_j; \overline{S}_j) - r_j^2 \right)^2, \qquad r \in [0, R_j] \tag{22}$$

where $R_j = \max_{p_i \in \pi_j} d_M(p, c_j; S_j)$ such that $\overline{r}_j^2 = \frac{1}{|\pi_j|} \sum_{p_i \in \pi_j} d_M^j(p, \overline{c}_j; \overline{S}_j)$. On an excellent initialization the positive definiteness of S_j is preserved. Eq. (16) can then be transformed into Eq. (23) as the solution. The summary of the KCMC algorithm is presented in Algorithm 1.

$$E_j^*(c_j^*, r_j^*; S_J^*) = argmin \sum_{p \in \pi_j} d(p, E(c_j, r_j; S_J)) \; ; \; c_j \in \mathbb{R}^2, \; r_j \in \mathbb{R}_+, \; S_j \in \mathbb{R}^{2 \times 2} \tag{23}$$

Fig. 7 presents the multi-ellipse fitting by the KCMC algorithm under the two explored touching-eggs configurations.

2.4. Multi-egg volume estimation

This study aims to accurately and efficiently compute the volume of each egg in a clutch of eggs based on the initially developed volume estimation model. For comparative analysis, the results of the two explored touching-eggs scenarios were compared in terms of the accuracy in volume estimation to the drainage method volume. The proposed multiple egg volume estimation system is summarized in Algorithm 2. In summary, the clusters c in the $A_{x,y}$ are computed based on C_v and C_x points evaluation and split-lines extraction technique. For each c, contour points $\mathscr{P}(\mathscr{C}; k)$ were extracted based on the Canny method (Biswas and Sil, 2012). After which a set E of k ellipses were fitted by KCMC algorithm on each cluster. γ_A, γ_E and γ_P of each E was extracted and applied as an input to the volume estimation model.

The accuracy of the estimated volume for each configuration was compared to the drainage method in terms of relative error, R-Squared (R^2) and $RMSE$. Additionally, Dependent T-Test was performed to analyze the differences between the drainage method volume (Vol_0), $Mod1$ estimated volume (Vol_1) $Mod2$ estimated volume (Vol_2), and $Mod3$ estimated volume (Vol_3) of the same egg. The Dependent T-Test generally compares the means of two related groups based on the same continuous dependent variable (Norušis, 2006). The normality of the data prior to the T-test was ascertained by the skewness value and skewness standard error values (Norušis, 2006). Note that no data transformation was performed in this study. All statistical computations
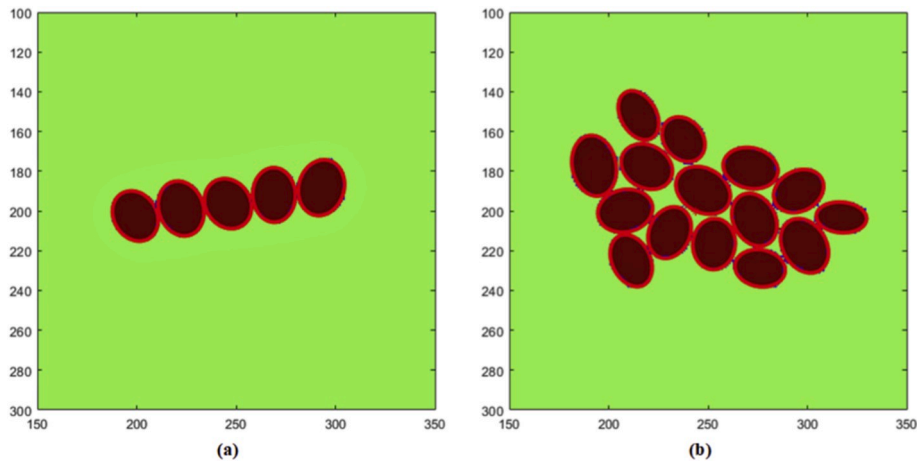

Fig. 7. Multi-ellipse fitting by KCMC algorithm on each egg after splitting in (a) simple touching configuration (*Mod2*), and (b) complex touching configuration (*Mod3*).

were performed using SPSS software package version 25.0 (SPSS Inc., Chicago, IL, USA).

3. Results

3.1. Dataset statistical description

A descriptive statistic of the entire dataset is given in Table 3 in terms of measures of central tendency and measures of variability (spread) in Vol_0. For the 1500 chicken eggs, it was established that the mean volume was 61.253 cm^3, with a median of 58.824 cm^3 ranging from 40.021 cm^3 (minimum) to 84.412 cm^3 (maximum). The dataset had a skewness of 0.066 cm^3 at a standard error of 0.225 cm^3

3.2. Volume estimation model evaluation

All model parameters of each modeling technique explored in his study are presented in Table 4. These regression model parameters are crucial factors that affect the overall performance of a model in terms of accuracy and efficiency. The GPR hyperparameters were computed by an automatic hyperparameter optimization technique that aims at minimizing the validation loss during the 10-fold cross-validation in the model training phase. Similarly, the SVR kernel function parameters were computed iteratively during the 10-fold cross-validation (kernel parameters resulting in the highest validation accuracy while effectively avoids underfitting and overfitting of the model and with a good generalization ability).

Additionally, for all the ANN networks, the number of neurons in the hidden layers was set to 10 (3-10-1 topology) to balance the computation time and the error term during model validation. The developed models were applied to the testing dataset to determine their accuracy in model testing. Table 5 presents the models' performance on the testing dataset in terms of R^2 and. RMSE

The Exponential GPR returned the best regression results of 0.984 R^2 at an RMSE of 1.175 cm^3, while Linear SVM had the lowest R^2 of 0.787 at an RMSE of 3.639 cm^3. Fig. 8 presents the linear regression plots for the Vol_0 against the estimated volumes (Vol_1, Vol_2 and Vol_3). All the Vol_1, Vol_2 and Vol_3 in $Mod2$ and $Mod3$ were computed based on the Exponential GPR model (best model).

It was established that the average relative error for Vol_1 in $Mod1$ was 3.515%, with a maximum and minimum of 4.801% and 0.374%, respectively, as presented in Table 6.

3.3. Touching-eggs splitting algorithm evaluation

The performance of the splitting algorithm was evaluated in terms of the splitting accuracy (object count) and the accuracy of Vol_2 and Vol_3 in comparison to Vol_0 for the same eggs. It can be observed that the introduced splitting technique accurately segmented all the eggs in the explored images of eggs in clutches, i.e., the number of image objects

Table 3
The descriptive statistics of the measures chicken eggs volume ($n = 1500$).

Descriptive statistics	Value (cm^3)
Minimum	40.021
Maximum	84.412
Range	44.391
1st quartile	55.882
Median	58.824
3rd quartile	69.853
Skewness	0.066
Mean	61.284
Standard error	0.225
Standard deviation	8.732
Variance	76.243

Table 4
The parameters of the developed Regression models.

SVR Kernel parameters	Scale (σ)	Degree (d)
Linear SVM	1.0842	–
Quadratic SVM	0.9253	2
Cubic SVM	0.9395	3
Fine Gaussian SVM	0.4300	–
Medium Gaussian SVM	1.7000	–
Coarse Gaussian SVM	6.9000	–

GPR Kernel parameters	length-scale (λ)	scale mixture (α)
Rational quadratic GPR	1.1391	0.0138
Squared exponential GPR	0.3129	–
Matern 5/2 GPR	0.4351	–
Exponential GPR	5.5756	–

ANN topology	Input – hidden layer – output	
Bayesian Regularization ANN	3-10-1	
Levenberg-Marquardt ANN	3-10-1	
Scaled Conjugate gradient ANN	3-10-1	

Table 5
The comparison of the performance of different regression models on the testing dataset (R-Squared (R^2) and RMSE).

Regression models	R-Squared (R^2)	RMSE
Linear SVM	0.787	3.639
Quadratic SVM	0.812	3.497
Cubic SVM	0.826	3.372
Fine Gaussian SVM	0.969	1.982
Medium Gaussian SVM	0.862	3.026
Coarse Gaussian SVM	0.818	3.376
Rational quadratic GPR	0.983	1.266
Squared exponential GPR	0.978	1.362
Matern 5/2 GPR	0.982	1.289
Exponential GPR	0.984	1.175
Bayesian Regularization ANN	0.954	1.618
Levenberg-Marquardt ANN	0.953	1.626
Scaled Conjugate gradient ANN	0.953	2.204

(after splitting) was equal to the observed number of eggs in all the images for both $Mod2$ and $Mod3$ as shown in Fig. 9. Additionally, to determine the performance of this introduced splitting technique with clutch size (effect of clutch size), the average relative error (in Vol_2 and Vol_3) for each clutch size was evaluated as presented in Fig. 10.

It was established that the performance of the introduced technique was invariant to the number of eggs per clutch. In $Mod2$ the highest and the least mean relative errors of 2.449% and 1.432% were observed when the clutch sizes were 7 and 6 eggs, respectively. However, for $Mod3$ had the highest, and the lowest mean relative errors of 2.988% and 1.778% were observed when the clutch size was 12 and 3 eggs, respectively.

Additionally, the introduced technique was evaluated based on the computational speed, as shown in Fig. 11. The least average computation time (1.562 s) was observed in $Mod2$ at the clutch size of 3 eggs, while the highest average computation time (11.098 s) was observed in $Mod3$ at the clutch size of 15 eggs. Furthermore, the average computation time for $Mod2$ was lower than that for $Mod3$ for all the clutch sizes. Thus, segmentation processing speed for $Mod2$ was higher than. $Mod3$

3.3.1. Simple egg-touching configuration

For the entire $Mod2$ dataset, Vol_2 was estimated at an R^2 of 0.981 with an RMSE of 1.080 cm^3, as presented in Fig. 8. The average relative error was 4.413% with a maximum and minimum of 6.261% and 0.933%, respectively, as shown in Table 5. Additionally, an evaluation was performed to determine the statistical differences between Vol_o, Vol_1, and Vol_2. By Dependent T-Test, there was a statistically significant difference ($p < 0.05$) between Vol_0 and Vol_2 and between Vol_1 and Vol_2.
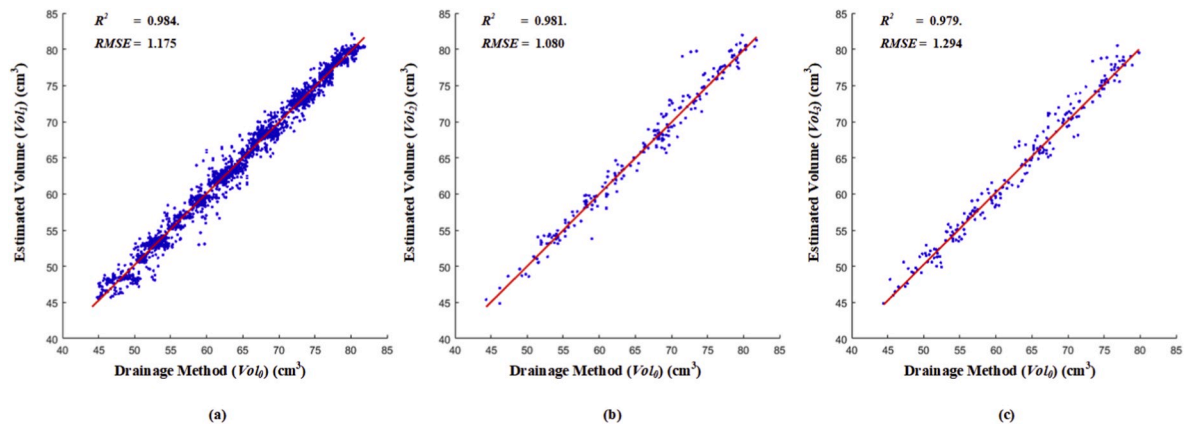
Fig. 8. The linear regression plots for the measured volume against the estimated volume, (a) drainage method (Vol_0) against the estimated volume for the entire testing dataset (Vol_1 in$Mod1$), (b) drainage method (Vol_0) against the estimated volume for the eggs in simple touching configuration (Vol_2 in$Mod2$), and (c) drainage method (Vol_0) against the estimated volume for the eggs in complex touching configuration (Vol_3 in$Mod3$).
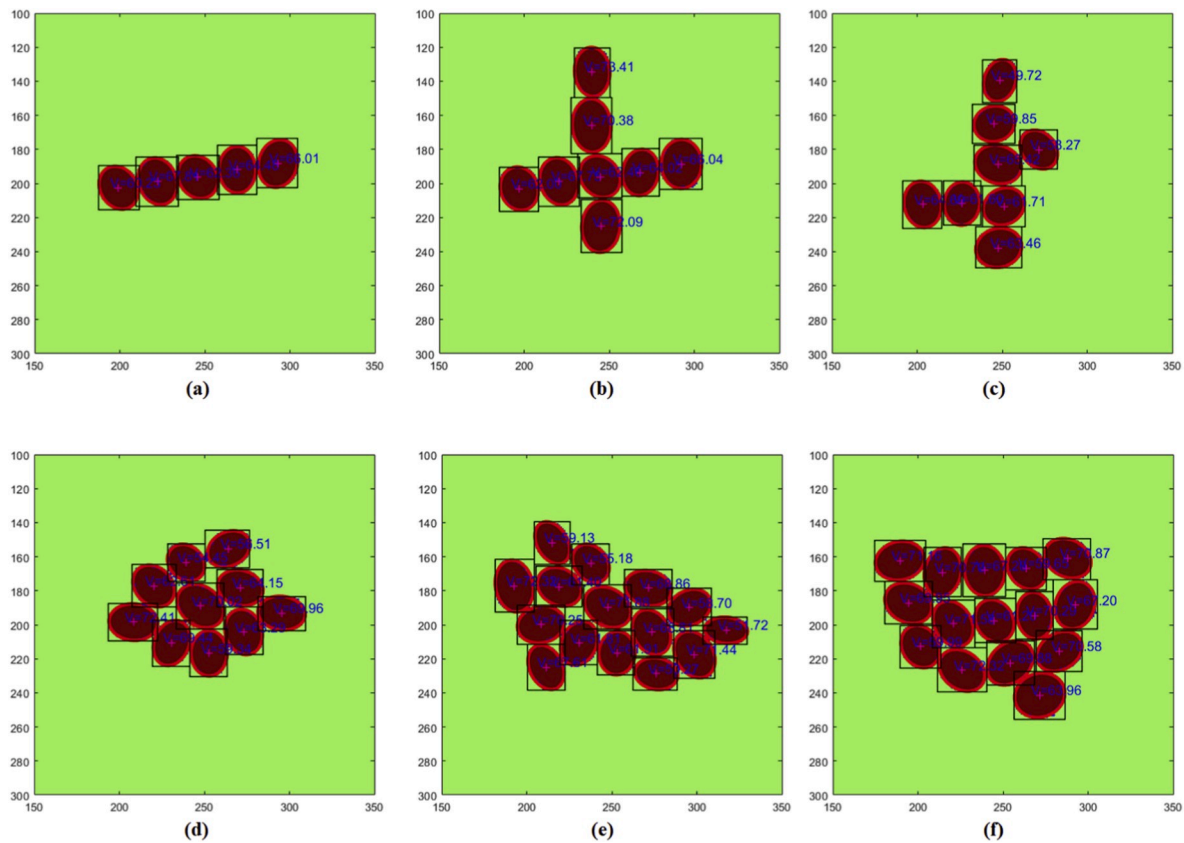

Fig. 9. The splitting and volume estimation results for different clutch configuration, (a), (b) and (c) simple touching-eggs configuration ($Mod2$), (d), (e) and (f) complex touching-eggs configuration ($Mod3$).

Table 6
The results of the chicken egg estimation under different modes of touching egg configuration.

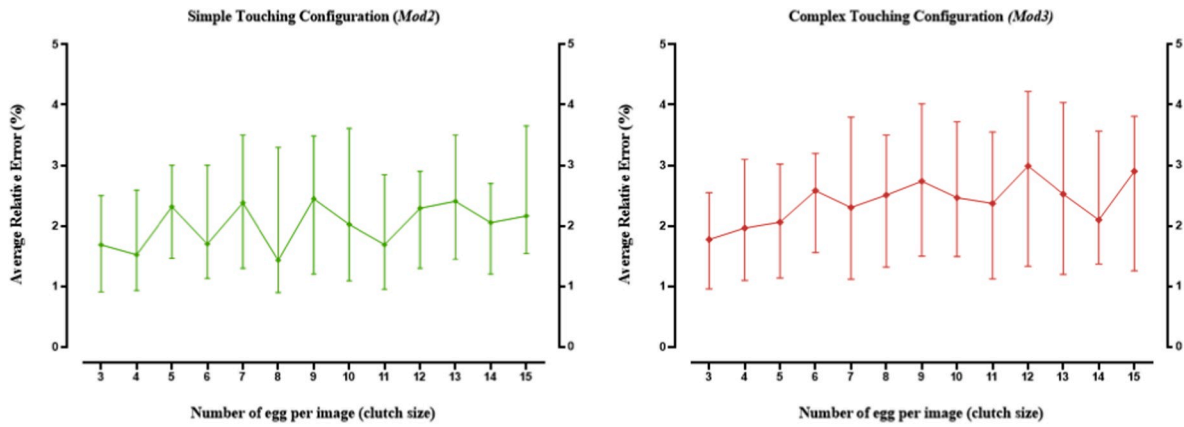| Egg touching configurations	R^2	RMSE (cm^3)	Relative error (%)			n
			Minimum	Maximum	Average	
$Mod1$	0.984	1.175	0.374	4.801	3.515	2250
$Mod2$	0.981	1.080	0.933	6.261	4.413	205
$Mod3$	0.979	1.294	0.776	7.285	5.659	205

Fig. 10. The Average Relative error per number of eggs in a clutch for both simple touching (*Mod*2) and complex touching (*Mod*3) configurations.
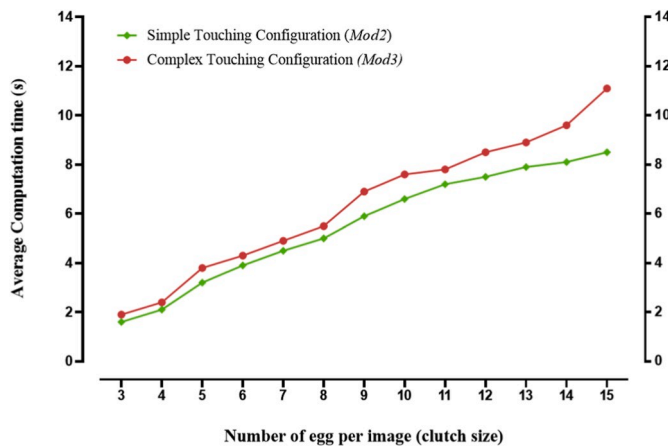

Fig. 11. A comparison of the proposed segmentation technique based on computation time in spitting of touching chicken eggs under both simple touching (*Mod*2) and complex touching (*Mod*3) configurations.

However, there was no statistically significant difference ($p < 0.05$) between Vol_0 and Vol_1 as shown in Table 6. It can be observed that Vol_2 was under-estimated by 1.561 cm^3 in comparison to Vol_0.

3.3.2. Complex egg-touching configuration

For the entire *Mod*3, Vol_3 was estimated at an R^2 of 0.979 with an *RMSE* of 1.294 cm^3, as presented in Fig. 8. The average relative error was 5.659%, with a maximum and minimum of 7.285% and 0.776%, respectively, as presented in Table 6.

A Dependent T-Test between all the volume groupings is presented in Table 7. It was established that there was no statistically significant difference ($p < 0.05$) between Vol_2 and Vol_3. However, there was a statistically significant difference ($p < 0.05$) between Vol_0 and Vol_3 and between Vol_1 and Vol_3 with an overall mean reduction of 2.088 cm^3 in Vol_3 in comparison to. Vol_0

Table 7
The statistical results of the measured volume (Vol_0) and the estimated volumes (Vol_1, Vol_2, and Vol_3) expressed in terms of mean and standard deviation.

Vol_0 (cm^3) mean± std	Vol_1 (cm^3) mean ± std	Vol_2 (cm^3) mean ± std	Vol_3 (cm^3) mean ± std
63.596 ± 8.932[a]	63.977 ± 9.101[a]	62.035 ± 8.462[b]	61.508 ± 8.794[b]

a,b mean ± std within a row, with no superscript in common, differ significantly.($p < 0.05$)

4. Discussion

This study introduces an automated chicken-egg volume prediction system that can be applied in a real production line system based on computer vision. A depth image pre-processing algorithm was developed as the initial step to segment the eggs from the background. After which a features extraction algorithm was applied to extract the egg shape image features. Based on previous studies (Soltani et al., 2015; Wang and Nguang, 2007; Zhang et al., 2016) of egg volume estimation, geometric features are often preferred due to their descriptive abilities. Therefore, in our study, egg image features were described by the three common shape geometric parameters γ_A, γ_E and γ_P.

A comparison of the developed models in Table 5 shows that the Exponential GPR outperformed all the other models. Additionally, it was established that all the GPR-based models outperformed all the SVR-based models, while only the Fine gaussian SVM outperformed the ANN-based models. This could be attributed to the ability of GPR models to handle uncertainty in noisy datasets due to their stochastic nature (Rasmussen, 2003), and good generalization ability on the testing dataset by the Fine gaussian SVM (Okinda et al., 2019).

The drainage method is always the primary technique of volume measurements of irregular objects or objects with varying densities. As already mentioned, the density of an egg is a function of storage time and ambient temperature. Therefore, an assumption of a constant chicken egg density values can yield errors in volume measurements. The results of this proposed study concurred with those of Wang and Nguang (2007) and Uyar and Erdoğdu (2009) in terms of volume estimation accuracy of 3.23% (percentage difference) and 3.15% (maximum percent error). The 3D approach by Zhang et al. (2016) reported an accuracy of 99%. Similar to the application of 3D scanners (Uyar and Erdoğdu, 2009), 3D reconstruction requires the acquisition of multi-angle images before a photometric approach, which would be quite challenging to be applied in real time production lines.

In an on-line production system, eggs move randomly in clutches. Therefore, a robust volume prediction system should have the ability to estimate the volume of each egg in any position (partial or no occlusion) along the production line. This study presents a touching-eggs splitting technique prior to volume estimation. The introduced splitting technique provided a solution to an egg occlusion problem. Splitting of partially occluded objects algorithms are often based on; watershed-based algorithms, global minimization-based methods, and shape information based algorithms (Bai et al., 2009). However, Watershed based algorithms are often inefficient without a strong gradient between objects due to occlusion (Bai et al., 2009). The global minimization-based algorithms have a limitation of complexity in obtaining markers with an increasing number of occluded objected (Bai et al., 2009). Shape information based algorithms perform occluded object splitting by analyzing object contour to detect concave and

convex points (Bai et al., 2009; Lin et al., 2014). However, the performance of these techniques is often affected by contour noise (Latecki and Lakämper, 1999; Wang et al., 2014), and imperfect ellipse like contours in the multi-ellipse fitting. However, an egg is always elliptical in nature. Therefore, a shape information-based algorithm was implemented in this study.

In shape representation, occlusion points are described by high curvature points on an object boundary (Laiche et al., 2014). Therefore, the task was to extract the high concave points along the shape contour as the occlusion points for split-lines extraction. In comparison to the study by Lin et al. (2014), they determined the high curvature points based on a curvature curve function, which required the transformation of the extracted curvature peaks to be invariant to rotation and translation. However, for the study by Bai et al. (2009), concave points were determined by a set threshold on the angles between two successive contour points. Our proposed study introduces an efficient, accurate determinant based technique for high curvature points extraction from contour primitives for noise invariance and a reduction in computational complexity. In $Mod2$ a maximum of two split-lines were required to segment a single egg from a clutch depending on the eggs position (edge position required one split-line, while mid positions required two split-lines). However, in $Mod3$ the number of split lines increased from one depending on the egg position in a clutch and the clutch size as presented in Fig. 6.

The proposed algorithm computation time was observed (Fig. 11) to increase with the clutch size because more eggs in an image introduce more shape structures. Hence, increased image complexity with reference to split lines extraction. In an industrial production line system, eggs follow each other at approximately 0.1 s. However, his proposed study reported a processing time of 2–12 s per image frame depending on the clutch size. Therefore, it can be applied in a farm laboratory based on this experimental setup. However, for this system to be applied in an industrial setting, a superior computing resource is required, because the processing speed of any computational system is always determined by the underlying computational resource (Hennessy and Patterson, 2011). Additionally, the frame rate of the Kinect camera can also be increased ($\leq$30 fps from Table 1) to further reduce the processing speed.

In an efficient splitting algorithm, the robustness and effectiveness of the technique are determined by the accuracy of the developed system with reference to the number of occluded objects. Fig. 10 shows that the average relative error after the splitting technique is independent of the clutch size, but only on the prior image processing operation. However, $Mod3$ relative errors were a little higher than those of $Mod2$. This can be attributed to the effect of multiple split-lines on the egg shape pixel points. Despite this, there was no statistically significant ($p < 0.05$) difference between Vol_2 and Vol_3 with an overall reduction of 1.943 cm^3 (maximum in $Mod2$) and 2.088 cm^3 ($Mod3$) in Vol_2 and Vol_3, respectively, compared to Vol_0. Therefore, the introduced system within an average error range of 4.413%–5.659% can accurately predict the volume of a chicken egg under partial occlusion (eggs in a clutch).

5. Conclusions

This study proposes a novel chicken-egg volume estimation system based on computer vision and machine learning techniques for eggs under no and partial occlusions. The proposed IR depth sensor system can be applied in a production line setting to predict the volume of eggs as a single object or under partial occlusion with minimum errors. However, IR depth sensors are limited to indoor applications due to their susceptibility to sunlight. Additionally, the system needs to be validated on different types of chicken eggs. Furthermore, a superior computing resource and a higher frame rate are recommended to improve the processing speed of the proposed system. Despite these shortcomings, the proposed technique achieved the objectives of this study in the splitting of chicken eggs under partial occlusion and volume estimation. It is of great importance to develop an accurate, efficient, and reliable

sorting and grading systems that can be applied in an in-line production system to reduce sorting time and labor costs. This system can be applied in any location along the production line. Additionally, this proposed system can be integrated with other quality detection systems such as cracked egg detection systems in chicken-egg grading and sorting systems. Furthermore, this technique can be applied to other axisymmetric agricultural products.

Author contribution

Cedric Okinda: Conceptualization, Methodology, Software, Validation, Original draft, Review & Editing. Yuwen Sun: Resources, Data curation, Formal analysis. Innocent Nyalala: Visualization, Methodology, Validation, Review & Editing. Tchalla Korohou: Methodology, Validation, Review & Editing. Samwel Opiyo: Methodology, Software, Validation, Review & Editing. Jintao Wang: Resources, Investigation, Methodology. Mingxia Shen: Supervision, Project administration, Funding acquisition.

Declaration of competing interest

All authors declare that they have no conflict of interest.

Algorithm 1
The k closest M-circle-centers algorithm (KCMC).

	Input: $A_{x,y}$
	Output: a set E of k ellipses
1	$[\pi_1, ..., \pi_k] = ComputeClusters(A_{x,y})$
2	**For** each π **do**
3	$[c, S] = findMcircleCenter(d_M)$
4	$r = computeRadius(d_M, p, c, S)$
5	$d = computeAlgebraicDist(p, c, r, S)$
6	$E(c, r, S) = fittEllipse(d, p, c, r, S)$
7	**end**

Algorithm 2
Multi-egg volume estimation algorithm.

	Input: $A_{x,y}$, Mdl
	Output: V of a E set of k ellipses
1	$[C_v, C_x] = ContourEvaluation(A_{x,y})$
2	$c = ExtractSplitlines(C_v, C_x)$
3	$\pi = ComputEdge(c)$
4	$E = KCMC (\pi)$
5	**for** each
	E **do**
6	$[\gamma_A, \gamma_E, \gamma_P] = ComputeFeatures(E)$
7	$V = RunModel(\gamma_A, \gamma_E, Mdl)$
8	**end**

References

Alexandratos, N., Bruinsma, J., 2012. World Agriculture towards 2030/2050: the 2012 Revision. ESA Working paper FAO, Rome. https://doi.org/10.22004/ag.econ.288998.

Asadi, V., Raoufat, M., Nassiri, S., 2012. Fresh egg mass estimation using machine vision technique. Int. Agrophys. 26, 229–234. https://doi.org/10.2478/v10247-012-0034-6.

Bai, X., Sun, C., Zhou, F., 2009. Splitting touching cells based on concave points and ellipse fitting. Pattern Recogn. 42, 2434–2446. https://doi.org/10.1016/j.patcog.2009.04.003.

Biswas, R., Sil, J., 2012. An improved canny edge detection algorithm based on type-2 fuzzy sets. Procedia Technol 4, 820–824. https://doi.org/10.1016/j.protcy.2012.05.134.

Chalidabhongse, T., Yimyam, P., Sirisomboon, P., 2006. 2D/3D vision-based mango's feature extraction and sorting. In: 2006 9th International Conference on Control, Automation, Robotics and Vision. IEEE, pp. 1–6. https://doi.org/10.1109/ICARCV.2006.345248.

Concha-Meyer, A., Eifert, J., Wang, H., Sanglay, G., 2018. Volume estimation of strawberries, mushrooms, and tomatoes with a machine vision system. Int. J. Food Prop. 21, 1867–1874. https://doi.org/10.1080/10942912.2018.1508156.

Cortes, C., Vapnik, V., 1995. Support-vector networks. Mach. Learn. 20, 273–297. https://doi.org/10.1007/BF00994018.

Eifert, J.D., Sanglay, G.C., Lee, D.-J., Sumner, S.S., Pierson, M.D., 2006. Prediction of raw produce surface area from weight measurement. J. Food Eng. 74, 552–556. https://doi.org/10.1016/j.jfoodeng.2005.02.030.

Fankhauser, P., Bloesch, M., Rodriguez, D., Kaestner, R., Hutter, M., Siegwart, R., 2015. Kinect v2 for mobile robot navigation: evaluation and modeling. In: 2015 International Conference on Advanced Robotics (ICAR). IEEE, pp. 388–394. https://doi.org/10.1109/ICAR.2015.7251485.

Friedman, J., 2018. An Algorithm for Finding Best Matches in Logarithmic Expected Time. SLAC National Accelerator Lab., Menlo Park, CA (United States).

Gerland, P., Raftery, A.E., Ševčíková, H., Li, N., Gu, D., Spoorenberg, T., Alkema, L., Fosdick, B.K., Chunn, J., Lalic, N., 2014. World population stabilization unlikely this century. Science 84 346, 234–237. https://doi.org/10.1126/science.1257469.

Goñi, S.M., Purlis, E., Salvadori, V.O., 2007. Three-dimensional reconstruction of irregular foodstuffs. J. Food Eng. 82, 536–547. https://doi.org/10.1016/j.jfoodeng.2007.03.021.

Guerrero-Peña, F.A., Vasconcelos, G.C., 2017. Object recognition under severe occlusions with a hidden Markov model approach. Pattern Recogn. Lett. 86, 68–75. https://doi.org/10.1016/j.patrec.2016.12.022.

Halır, R., Flusser, J., 1998. Numerically stable direct least squares fitting of ellipses. In: Proc. 6th International Conference in Central Europe on Computer Graphics and Visualization. WSCG. Citeseer, pp. 125–132.

Hennessy, J.L., Patterson, D.A., 2011. Computer Architecture: a Quantitative Approach. Elsevier.

Jana, A., 2012. Kinect for Windows SDK Programming Guide. Packt Publishing Ltd.

Javadikia, P., Dehrouyeh, M.H., Naderloo, L., Rabbani, H., Lorestani, A.N., 2011. Measuring the weight of egg with image processing and ANFIS model. In: International Conference on Swarm, Evolutionary, and Memetic Computing. Springer, pp. 407–416. https://doi.org/10.1007/978-3-642-27172-4_50.

Jin, Y.H., Lee, K.T., Lee, W.I., Han, Y.K., 2011. Effects of storage temperature and time on the quality of eggs from laying hens at peak production. AJAS (Asian-Australas. J. Anim. Sci.) 24, 279–284. https://doi.org/10.5713/ajas.2011.10210.

John-Jaja, S.A., Udoh, U.H., Nwokolo, S.C., 2016. Repeatability estimates of egg weight and egg-shell weight under various production periods for Bovan Nera Black laying chicken. Beni-Suef Univ. J. Basic Appl. Sci. 5, 389–394. https://doi.org/10.1016/j.bjbas.2016.11.001.

Jun, K., Kim, S.J., Ji, H.W., 2018. Estimating pig weights from images without constraint on posture and illumination. Comput. Electron. Agric. 153, 169–176. https://doi.org/10.1016/j.compag.2018.08.006.

Kongsro, J., 2014. Estimation of pig weight using a Microsoft Kinect prototype imaging system. Comput. Electron. Agric. 109, 32–35. https://doi.org/10.1016/j.compag.2014.08.008.

Laiche, N., Larabi, S., Ladraa, F., Khadraoui, A., 2014. Curve normalization for shape retrieval. Signal Process. Image Commun. 29, 556–571. https://doi.org/10.1016/j.image.2014.01.009.

Latecki, L.J., Lakämper, R., 1999. Convexity rule for shape decomposition based on discrete contour evolution. Comput. Vis. Image Understand. 73, 441–454. https://doi.org/10.1006/cviu.1998.0738.

Lee, D.-J., Xu, X., Eifert, J.D., Zhan, P., 2006. Area and volume measurements of objects with irregular shapes using multiple silhouettes. Opt. Eng. 45, 27202. https://doi.org/10.1117/1.2166847.

Lesnierowski, G., Stangierski, J., 2018. What's new in chicken egg research and technology for human health promotion?-A review. Trends Food Sci. Technol. 71, 46–51. https://doi.org/10.1016/j.tifs.2017.10.022.

Lin, P., Chen, Y.M., He, Y., Hu, G.W., 2014. A novel matching algorithm for splitting touching rice kernels based on contour curvature analysis. Comput. Electron. Agric. 109, 124–133. https://doi.org/10.1016/j.compag.2014.09.015.

Mao, K.Z., Zhao, P., Tan, P.-H., 2006. Supervised learning-based cell image segmentation for p53 immunohistochemistry. IEEE Trans. Biomed. Eng. 53, 1153–1163. https://doi.org/10.1109/TBME.2006.873538.

Marošević, T., Scitovski, R., 2015. Multiple ellipse fitting by center-based clustering. Croat. Oper. Res. Rev. 6, 43–53. https://doi.org/10.17535/crorr.2015.0004.

Norušis, M.J., 2006. SPSS 14.0 Guide to Data Analysis. Prentice Hall, Upper Saddle River, NJ.

Nyalala, I., Okinda, C., Nyalala, L., Makange, N., Chao, Q., Chao, L., Yousaf, K., Chen, K., 2019. Tomato volume and mass estimation using computer vision and machine learning algorithms: cherry tomato model. J. Food Eng. 263, 288–298. https://doi.org/10.1016/j.jfoodeng.2019.07.012.

Okinda, C., Lu, M., Liu, L., Nyalala, I., Muneri, C., Wang, J., Zhang, H., Shen, M., 2019. A machine vision system for early detection and prediction of sick birds: a broiler chicken model. Biosyst. Eng. 188, 229–242. https://doi.org/10.1016/j.biosystemseng.2019.09.015.

Okinda, C., Lu, M., Nyalala, I., Li, J., Shen, M., 2018. Asphyxia occurrence detection in sows during the farrowing phase by inter-birth interval evaluation. Comput. Electron. Agric. 152, 221–232. https://doi.org/10.1016/j.compag.2018.07.007.

Pastrana, J.C., Rath, T., 2013. Novel image processing approach for solving the overlapping problem in agriculture. Biosyst. Eng. 115, 106–115. https://doi.org/10.1016/j.biosystemseng.2012.12.006.

Phate, V.R., Malmathanraj, R., Palanisamy, P., 2019. Classification and weighing of sweet lime (Citrus limetta) for packaging using computer vision system. J. Food Meas. Charact. 13, 1451–1468. https://doi.org/10.1007/s11694-019-00061-3.

Quinonero-Candela, J., Rasmussen, C.E., Williams, C.K.I., 2007. Approximation methods for Gaussian process regression. Large-scale kernel Mach 203–224. https://doi.org/10.7551/mitpress/7496.003.0011.

Rashidi, M., Gholami, M., 2011. Prediction of egg mass based on geometrical attributes. Agric. Biol. J. N. Am. 2, 638–644. https://doi.org/10.5251/abjna.2011.2.4.638.644.

Rasmussen, C.E., 2003. Gaussian processes in machine learning. In: Summer School on Machine Learning. Springer, pp. 63–71. https://doi.org/10.1007/978-3-540-28650-9_4.

Sabliov, C.M., Boldor, D., Keener, K.M., Farkas, B.E., 2002. Image processing method to determine surface area and volume of axi-symmetric agricultural products. Int. J. Food Prop. 5, 641–653. https://doi.org/10.1081/JFP-120015498.

Şalvarcı, Ü.B., Ayten, U.E., 2017. Distance independent weight estimation of eggs from images using artificial neural networks. In: 2017 25th Signal Processing and Communications Applications Conference (SIU). IEEE, pp. 1–4. https://doi.org/10.1109/SIU.2017.7960637.

Samarasinghe, S., 2016. Neural Networks for Applied Sciences and Engineering: from Fundamentals to Complex Pattern Recognition. Auerbach publications.

Siswantoro, J., Prabuwono, A.S., Abdullah, A., 2014. Volume measurement algorithm for food product with irregular shape using computer vision based on Monte Carlo method. J. ICT Res. Appl. 8, 1–17. https://doi.org/10.5614/itbj.ict.res.appl.2014.8.1.1.

Soltani, M., Omid, M., Alimardani, R., 2015. Egg volume prediction using machine vision technique based on pappus theorem and artificial neural network. J. Food Sci. Technol. 52, 3065–3071. https://doi.org/10.1007/s13197-014-1350-6.

Statista, 2019. Global Egg Production from 1990 to 2017 (In 1,000 Metric Tons).

Sun, K.B., Super, B.J., 2005. Classification of contour shapes using class segment sets. In: 2005 IEEE Computer Society Conference on Computer Vision and Pattern Recognition (CVPR'05). IEEE, pp. 727–733. https://doi.org/10.1109/CVPR.2005.98.

Thipakorn, J., Waranusast, R., Riyamongkol, P., 2017. Egg weight prediction and egg size classification using image processing and machine learning. In: 2017 14th International Conference on Electrical Engineering/Electronics, Computer, Telecommunications and Information Technology (ECTI-CON). IEEE, pp. 477–480. https://doi.org/10.1109/ECTICon.2017.8096278.

United Nations, 2010. UNECE Standard Egg-1.

Uyar, R., Erdoğdu, F., 2009. Potential use of 3-dimensional scanners for food process modeling. J. Food Eng. 93, 337–343. https://doi.org/10.1016/j.jfoodeng.2009.01.034.

Vivek Venkatesh, G., Iqbal, S.M., Gopal, A., Ganesan, D., 2015. Estimation of volume and mass of axi-symmetric fruits using image processing technique. Int. J. Food Prop. 18, 608–626. https://doi.org/10.1080/10942912.2013.831444.

Wang, T., Nguang, S., 2007. Low cost sensor for volume and surface area computation of axi-symmetric agricultural products. J. Food Eng. 79, 870–877. https://doi.org/10.1016/j.jfoodeng.2006.01.084.

Wang, X., Feng, B., Bai, X., Liu, W., Latecki, L.J., 2014. Bag of contour fragments for robust shape classification. Pattern Recogn. 47, 2116–2125. https://doi.org/10.1016/j.patcog.2013.12.008.

Williams, C.K.I., Rasmussen, C.E., 2006. Gaussian Processes for Machine Learning. MIT press Cambridge, MA. https://doi.org/10.7551/mitpress/7496.003.0011.

Xu, Y., Imou, K., Kaizu, Y., Saga, K., 2013. Two-stage approach for detecting slightly overlapping strawberries using HOG descriptor. Biosyst. Eng. 115, 144–153. https://doi.org/10.1016/j.biosystemseng.2013.03.011.

Zhang, D., Lu, G., 2004. Review of shape representation and description techniques. Pattern Recogn. 37, 1–19. https://doi.org/10.1016/j.patcog.2003.07.008.

Zhang, G., Jayas, D., White, N., 2005. Separation of touching grain kernels in an image by ellipse fitting algorithm. Biosyst. Eng. 92, 135–142. https://doi.org/10.1016/j.biosystemseng.2005.06.010.

Zhang, W., Wu, X., Qiu, Z., He, Y., 2016. A novel method for measuring the volume and surface area of egg. J. Food Eng. 170, 160–169. https://doi.org/10.1016/j.jfoodeng.2015.08.025.